


ALBA Project Document No:	Page: 1/20
AAD-SR-ID-AN-0166	Rev. No. : 1.0

	ACCELERATOR DIVISION Insertion Devices Section			
	ALBA Project Document No.	EDMS Document No.	Created: 21.09.06	Page: 1/20
AAD-SR-ID-AN-0166		Modified: 26.03.07	Rev. No.: 2.0	

Annex A

Conceptual magnetic design of the conventional Multipole wiggler MPW-80 for ALBA

Abstract

In this document we specify the main magnetic parameters for a MPW80 wiggler to be used in EXAFS beamline, as well as a conceptual design and magnetic performance of the device obtained by simulation.

<i>Prepared by:</i> J. Campmany J. Marcos Z. Martí	<i>Checked by:</i> D. Einfeld	<i>Approved by:</i> D. Einfeld
<i>Authorship:</i> J. Campmany		
<i>Distribution list:</i>		

Table of Contents

1. Introduction.....	3
2. Insertion device basics	3
3. Strategy of optimization	4
4. End sections determination and analysis of end effects	6
4.1. Model for end sections.....	6
4.2. Fringe field	8
4.3. Integrated Multipoles (Angular kick).....	8
5. Analysis of calculated fields at minimum gap.....	10
5.1. Longitudinal distribution of magnetic flux density B	10
5.2. Transverse roll off.....	11
5.3. Electron Orbit	12
6. Analysis of Gap Dependent Wiggler Parameters	13
6.1. Constraints for the 1st and 2nd field integrals along the wiggler.....	13
6.2. Variation of first field integral with gap.....	14
6.3. Variation of first field integral with gap.....	14
6.4. Maximum field	15
6.5. Forces.....	16
7. Demagnetizing fields.....	16
8. Magnetic material.....	19
9. Tolerances.....	19
10. Magnetic parameters of wiggler W80.....	20

Record of Changes

<i>Rev. No.</i>	<i>Date</i>	<i>Pages</i>	<i>Description of changes</i>
Draft 1.0	21.09.2006	****	Initial release
2.0	26.03.2007	****	Approved version

1. Introduction

In this paper we present the conceptual magnetic design of the conventional wiggler to be installed at ALBA EXAFS beamline. The main parameters (Maximum field, K value, length and period) have been derived from user's requirements:

- Maximum flux between 2 and 20 keV through a vertical aperture of 250 μ rad and a horizontal aperture of 1.5 mrad, for currents up to 400 mA.
- Maximum power into the monochromator: 700 W in the ranges 0-7 keV, 7-20 keV and 20-50 keV)

According to that specification, the main parameters of this insertion device are shown in Table 1 below.

Table 1. Main parameters for the ID feeding the EXAFS beamline.

Magnitude	Value
Magnetic length of the device	1 m
Period length	80 mm
K value to be used at 100 mA of electron current	12.976 (at 12.5 mm gap)
K value to be used at 400 mA of electron current	9.328 (at 17.95 mm gap)

The aim in this paper is to present the detailed magnetic design fulfilling both the user's specifications and the following criteria:

- Feasibility regarding materials, structures and dimensions.
- The amount of magnetic material to be used should be minimized as much as possible.
- The roll off should be equal or less than 1% at ± 20 mm
- Field integrals should be null or near to zero at two working gaps: 12.5 mm and ~ 18 mm.
- Mechanical structure should be designed to bore the forces generated by the undulator.

2. Insertion device basics

We choose a symmetric device because in this way, if the first integral is zero, then the second integral is also zero. So, when fitting the pole ends in order to reduce the first integral, the second will also trend to zero.

With respect to the materials, we have used in simulation the NdFeB material built-in in Radia with a remanent field $B_r = 1.4$ T. This type of material can be found in the market from a number of suppliers, as shown in Table 2.

Table 2. Possible commercial materials to be used for W80 device.

Supplier	Commercial name	B_r [T]	H_{CB} [kA/m]	H_{CJ} [kA/m]
Vacuumschmelze	VACODYM 745 HR	>1.40	>1065	>1115
	VACODYM 722 HR	>1.42	>835	>975
NEOMAX	Neomax 50BH	>1.39	>1050	>1114
	Neomax 52	>1.42	>835	>875
NEOREM	Neorem 5o3i	>1.38	>910	>950

With respect to the pole material, we have used the RADIA embedded Vanadium Permendur cobalted steel.

3. Strategy of optimization

In order to obtain the desired performance within the above criteria, the optimization process has been applied in two steps. (1) A model for the central period was constructed for optimizing the K value, amount of magnetic material, and transverse roll off. (2) A complementary model has been used for the optimization of the end field terminations and evaluation of the electron trajectory to ensure null first and second integrals at two gaps corresponding to two working K values derived in [1].

At the first step, we have simulated the magnetic behaviour of a 2.5 period wiggler (thus, a symmetric wiggler) using the RADIA code [2]. The free parameters of the model to be optimized have been: width and height of magnetic blocks, width and height of poles, and ratio between pole and magnetic block lengths. So, we have worked in a 5-D space parameter.

The merit function describing the goodness of each wiggler characterized by a set of 5 parameters has been defined as:

$$G = |B_0 - B_{\max \text{ teor}}| + |\text{rolloff} - 0.01| + |w \cdot h \cdot 10^{-7}|$$

where $B_0 = 1.7366$, $B_{\max \text{ teor}}$ is the maximum field in the centre of the wiggler calculated with RADIA from input parameters, *rolloff* is the field difference ratio at 20 mm off-axis in transversal X direction,

and w and h are the width and height of the magnetic blocks. The minimization of the merit function pushes towards the block with the minimum area ($w \cdot h$) providing a rolloff ca. 1% at ± 20 mm and a maximum field in the centre ca. 1.74 T.

The result of the optimization is given in Table 3 below.

Table 3. Central cell for the conventional W80

Magnitude	Value
Magnetic block width	109.6 mm
Magnetic block heigh	56.2 mm
Magnetic block thickness	26.6 mm
Pole width	75.2 mm
Pole heigh	43.3 mm
Pole block thickness	13.4 mm
Pole chamfer side width	4 mm
Magnet block chamfer side width	5 mm
Ratio pole/period lengths	0.335

Magnets and poles have been modelled with chamfers as shown in Figure 1. The location of electron beam is $x=y=z=0$

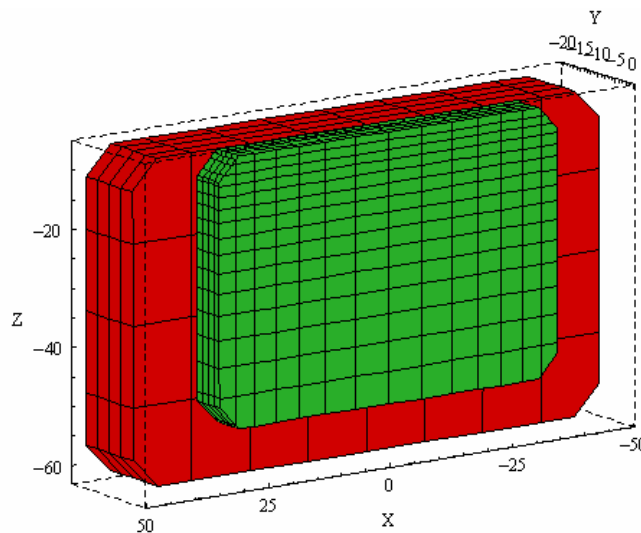


Figure 1. Shape of magnet block (red) and pole (green) optimized for W80.

For a wiggler built according to central period parameters given in Table 3, the K operational values given in Table 1 are reached with gap values of 12.5 mm and ~18 mm respectively. This are the operational gaps at which the device is foresee to be used.

4. End sections determination and analysis of end effects

In order to null the field integral along the longitudinal axis of the insertion device at both operational gaps, we optimized the end sections. In addition to that, we have also imposed as an additional constraint that the variation of the field integral with gap should be as small as possible.

4.1. Model for end sections

The optimization has been done with a model with 2.5 periods. Once solved, the optimized parameters have been applied with success to the full device to cross-check the validity of the optimization.

The end sections consist in two magnet block – permendur pole pairs. The width of poles and magnet blocks are the same of the central pole, whilst its height is reduced to $2/3$ and $1/3$ respectively from that of the central pole and magnet block, in order to smoothly decrease the end field peaks. In order to make the optimization, we have left 4 free parameters: the length of both poles (var2 and var4), and the separation between both poles and their magnetic blocks (var1 and var3) as shown in Figure 2.

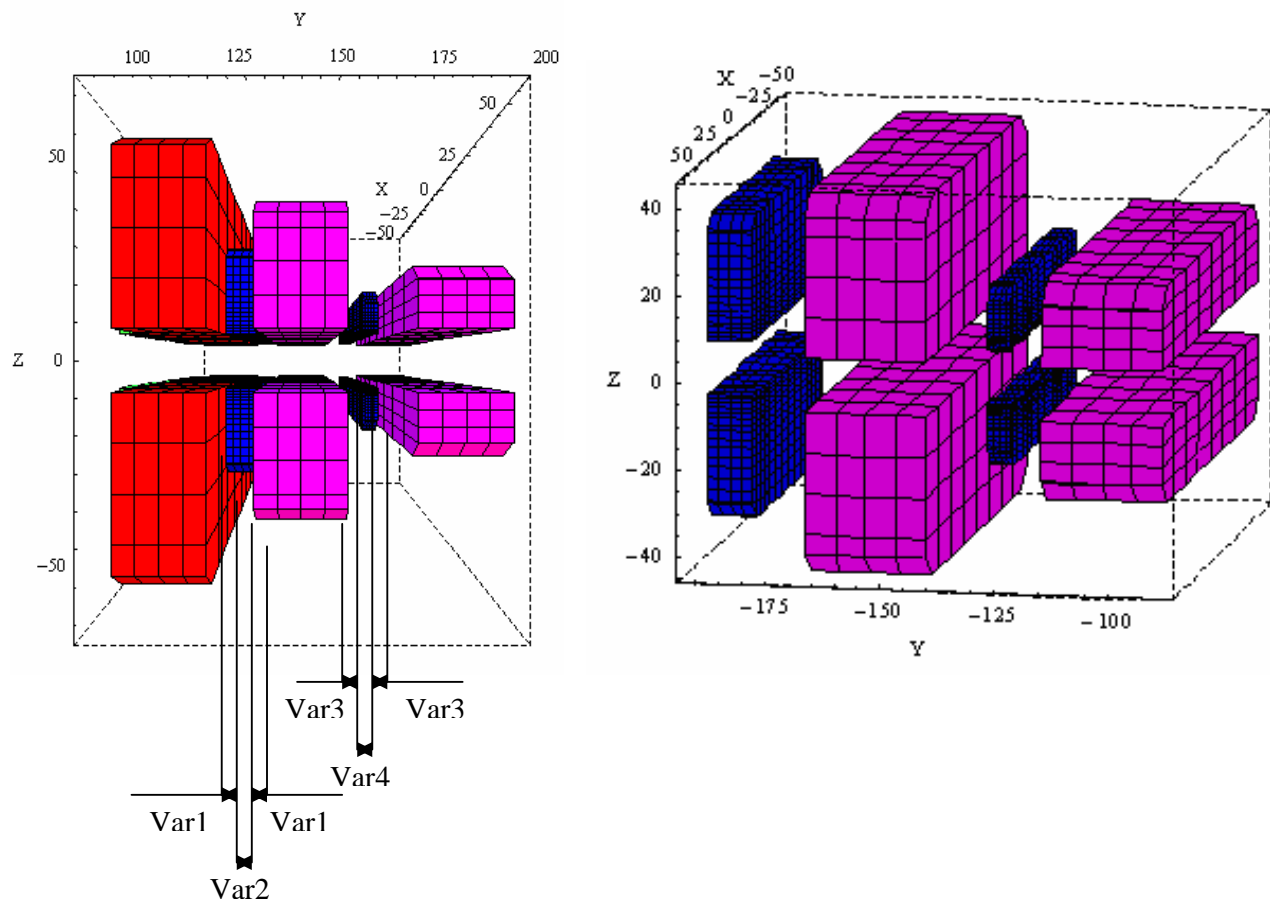


Figure 2. Model used for the end sections. Free parameters are var1, var2, var3 and var4.

In order to find the values of the free parameters that minimize the field integral at operational gaps, we have also introduced the constraint that maximum field integral variation with gap between minimum gap and fully open gap should also be small. In particular, the merit function which is minimized in the process has been defined as:

$$\mathcal{E} = |I_{closed}| + |I_{open}| + \frac{|I_{gap1}| + |I_{gap2}|}{10}$$

In the previous expressions, $gap_{closed} = 12.5$ mm, $gap_{open} = 17.95$ mm and I_{gap1} and I_{gap2} are two gaps within them, in our particular case, $gap_{gap1} = 14.0$ mm and $gap_{gap2} = 20.0$ mm. The contribution of the field integrals at these two gaps to the error function has been considered 10 times less than the contribution of the field integrals at both operational gaps. In this way we stress the optimization to fix null field integrals at operational gaps, and low values for the others.

We have used the model shown in Figure 3 below.

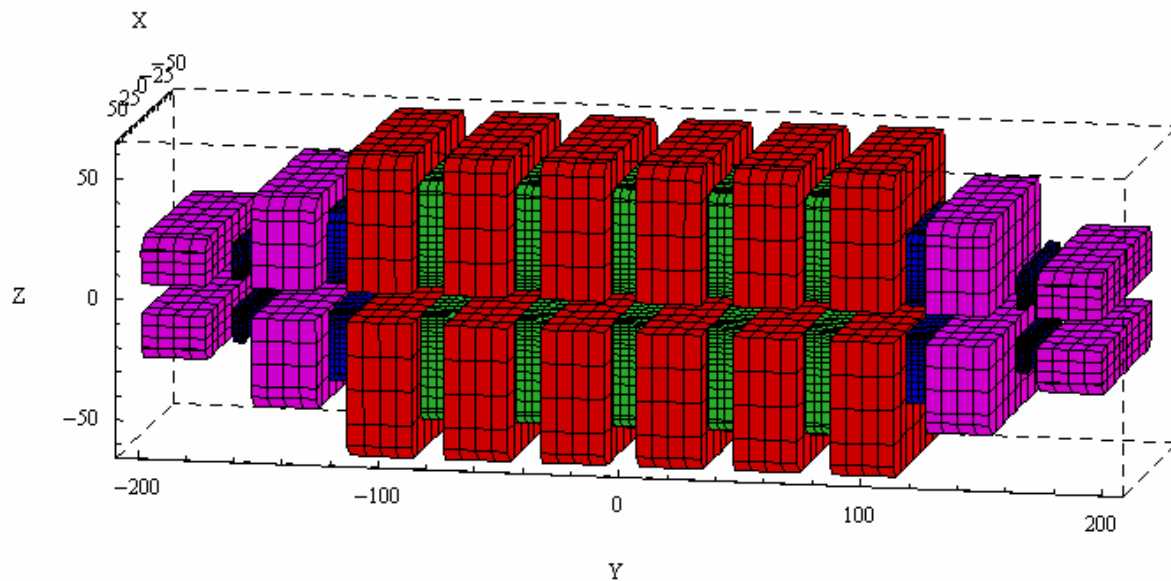


Figure 3. Model of the wiggler (4,5 periods) used to optimize the end section.

The optimum values of free parameters to minimize the field integral on axis are shown in Table4.

Table 4. End sections for W80

Magnitude		Value
Free space between pole 1 and magnetic blocks	Var1	1.505 mm
Length of pole 1	Var2	10.041 mm
Free space between pole 2 and magnetic blocks	Var3	7.649 mm
Length of pole 2	Var4	4.226 mm

The field integrals at the operational gaps are shown in Table 5.

Table 5. Field integrals for both operational gaps

Magnitude	Value
12.50 mm	0.0 G·cm
17.95 mm	12.4 G·cm

Full evolution of first field integral with gap is given in section 6.2 and Figure 11. Please note that the field integral values are given without correction coils. With correction coils these values should be both null.

4.2. Fringe field

In order to determine the total magnetic length of the wiggler we have to take into account that the field on the axis orbit does not null just outside the magnetic structure, but it presents some decay along a tail. In Figure 4 below we show this tail. The magnetic induction is of the order of the Earth field at 280 mm away from the magnetic blocks edge.

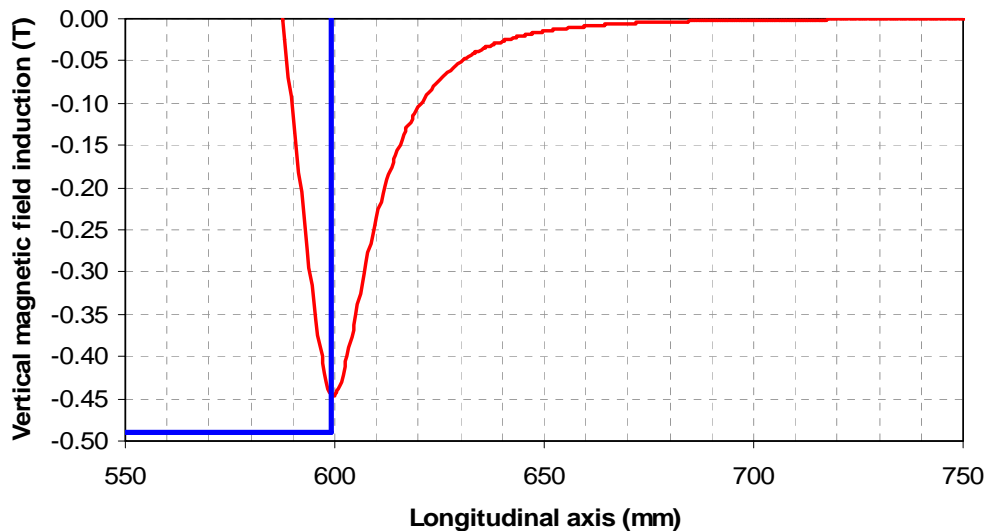


Figure 4. Fringe field at the edge of the wiggler. Blue line shows the physical end of the last magnetic block (including end sections), and red line represents the vertical magnetic field induction decay. Horizontal axis is referred to the centre of the wiggler.

4.3. Integrated Multipoles (Angular kick)

As a result of the optimization of pole sections, the magnetic field integral along the axis undulator is zero at both operational gaps. However, out from axis, the integral versus the transversal distance grows up according to a curve that can be developed using Taylor expansion. The coefficients of such expansion are the integrated multipoles of the device, which determine the angular kick of any particle

off-orbit. The integrated field integral is shown in Figure 5. In Table 6 we show the coefficients found in the Taylor expansion within the ± 20 mm around the axis.

Table 6. Integrated multipoles of W80 ideal model

Multipole	Value
Dipole	1.6 G-cm
Quadrupole	$4.5 \cdot 10^{-8}$ G
Sextupole	31 G/cm
Octupole	$8.9 \cdot 10^{-9}$ G/cm ²
Decapole	1.4 G/cm ³
Dodecapole	$-3.6 \cdot 10^{-9}$ G/cm ⁴

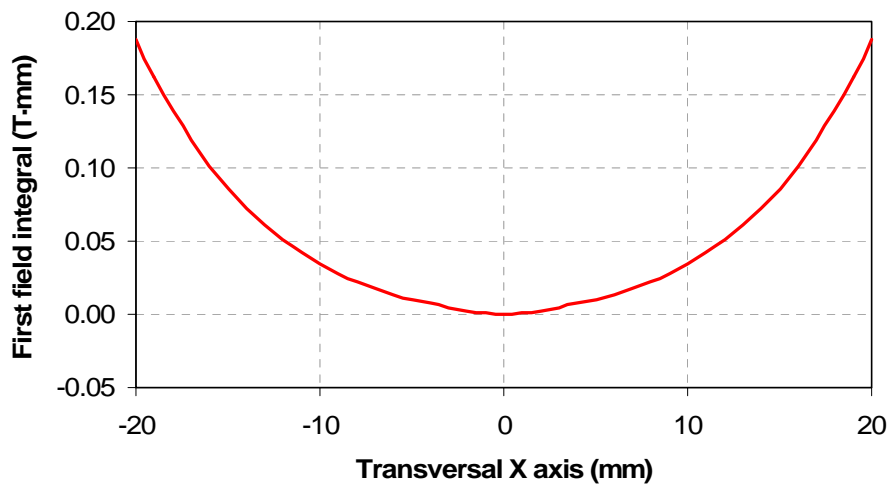
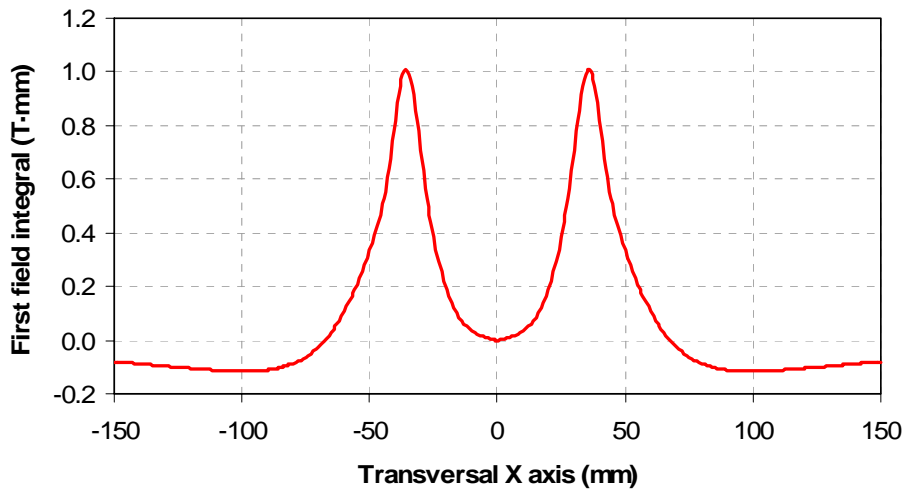


Figure 5: First field integral over a transverse width of ± 150 mm (top) and ± 20 mm (bottom) in the wiggler magnetic midplane at minimum gap

As it can be observed from Figure 5, the first field integral with respect to transversal X axis (mm) presents a clear symmetry and therefore the major multipolar components are the sextupole and the decapole.

5. Analysis of calculated fields at minimum gap

5.1. Longitudinal distribution of magnetic flux density B

The optimization of the central period has been done using first a small model with 2.5 periods. Then, the optimized parameters have been introduced in a new optimization round using the full model with 12.5 periods. In Figures 6 and 7 we show the vertical magnetic flux density along the longitudinal axis at the minimum gap. The device is symmetric, so making zero the second field integral also nulls the first field integral.

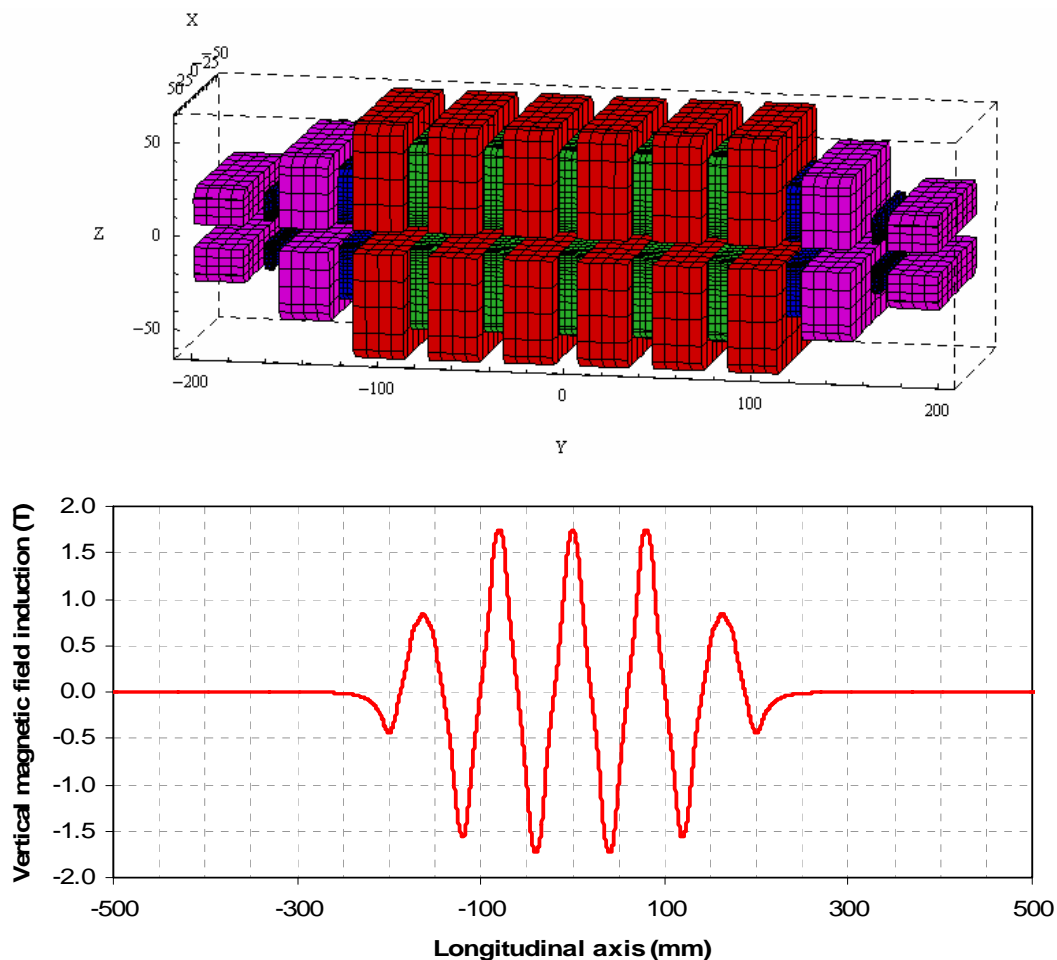


Figure 6. The 2,5 period model of W80 and the vertical magnetic induction on axis. The maximum field achieved is 1.74 T

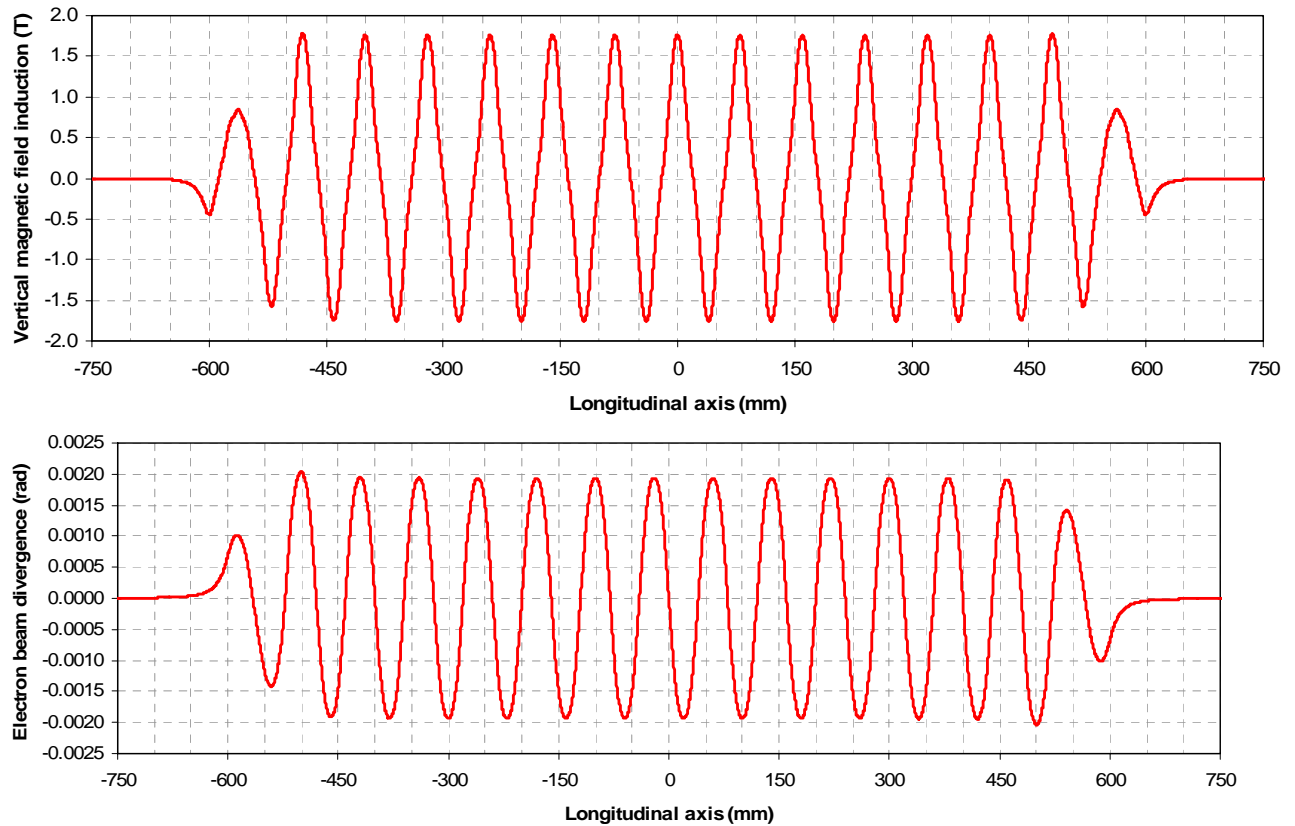


Figure 7. The vertical magnetic induction on axis, as well as the divergence induced in the electron beam calculated for the full model of W80.

From the simulated vertical magnetic induction on axis it can be calculated the total power emitted by the device, including that produced at edges. The total power is 1.40 kW. Note that this power is slightly lower than that calculated with the approximated formulae that considers a perfect sinusoidal magnetic field: $P = 0.6328 \cdot E^2 \cdot B_0^2 \cdot L \cdot I$, which gives a total emitted power of 1.51 kW.

5.2. Transverse roll off

In Figures 8 and 8 we show the roll-off of the field in the transversal horizontal axis.

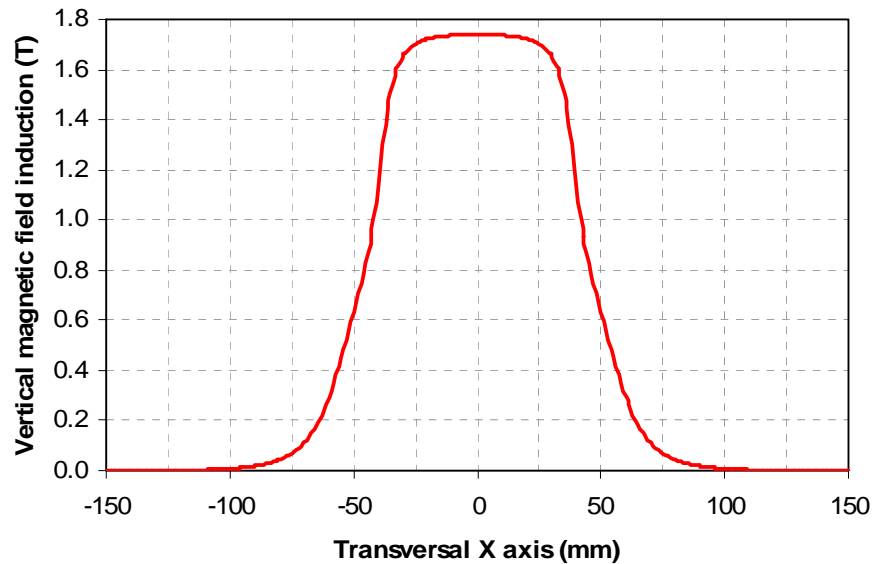


Figure 8. Vertical magnetic induction B_y versus transversal x direction at 12.5 mm gap.

According to the constraints introduced in the optimization, it is guaranteed that the roll off at ± 20 mm from the nominal orbit is $\sim 1\%$, as Figure 5 details.

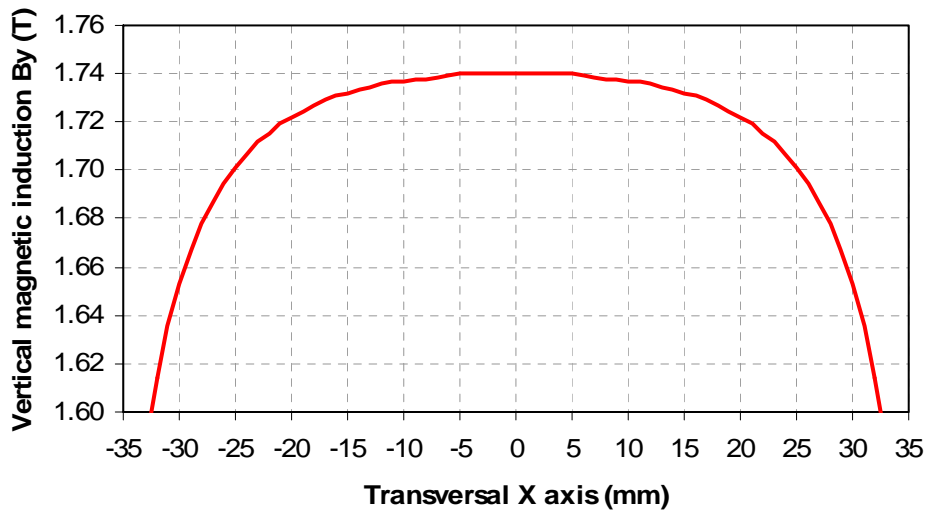


Figure 9. Detail of vertical magnetic induction B_y versus transversal x direction near nominal orbit at 12.5 mm nominal gap.

5.3. Electron Orbit

The end sections are designed to minimize the average model offset and exit angle of the electron orbit with respect to the centerline of the undulator. The orbit was averaged over a full period to better show the offset and angle of the electron in the central section. Figure 10 shows a graph of the electron

trajectory for a full wiggler. Note that the average deviation in the centre of the wiggler is 30 μm , which should be taken into account to align the beam-line.

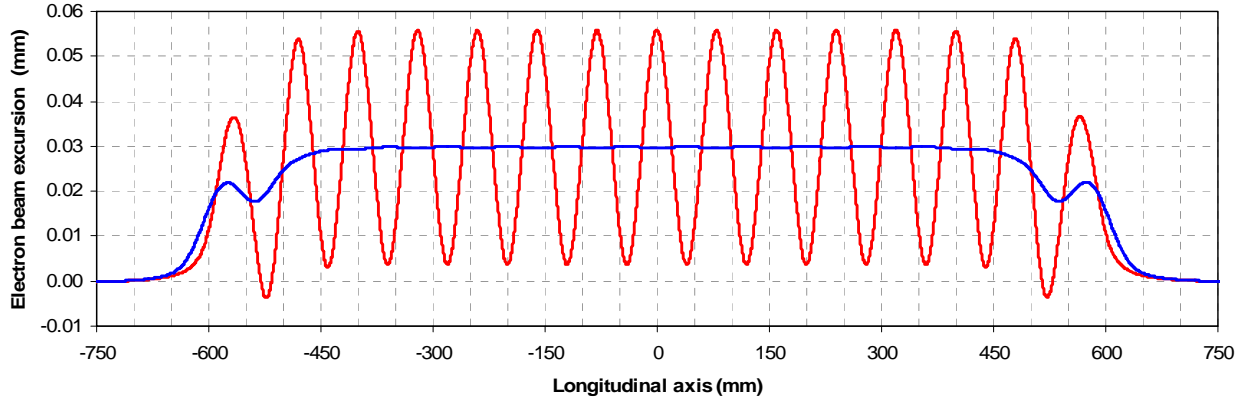


Figure 10: Electron orbit along the undulator axis over a length of ± 500 mm at 3 GeV for full wiggler W80 (12,5 periods). Blue line is the averaged trajectory. Note that the end sections break the periodicity.

6. Analysis of Gap Dependent Wiggler Parameters

The wiggler W80 to be used for the X-Ray Absorption Spectroscopy beam-line should be used in two operational gaps, so the dependence of the parameters affecting the beam orbit should be studied.

6.1. Constraints for the 1st and 2nd field integrals along the wiggler

In order to roughly evaluate the behaviour of the wiggler from the point of view of accelerator physics, we assume a closed orbit distortion around the ring circumference equal to 1/10 of the rms beam size over a full gap range of 12.5 to 20 mm. Using the expressions given below, the constraints for the first and second field integrals are:

$$I_x [G \cdot cm] \leq 21E [GeV] \sqrt{\frac{\varepsilon_x [nm]}{\beta_x [m]}} \sin(\pi \nu_x)$$

$$I_z [G \cdot cm] \leq 21E [GeV] \sqrt{\frac{\varepsilon_z [nm]}{\beta_z [m]}} \sin(\pi \nu_z)$$

$$J_x [G \cdot cm^2] \leq 1100E [GeV] \sqrt{\varepsilon_x [nm] \beta_x [m]}$$

$$J_z [G \cdot cm^2] \leq 1100E [GeV] \sqrt{\varepsilon_z [nm] \beta_z [m]}$$

In the above expressions we have the variables I , J , E , ε , β , ν , which are respectively the first field integral, second field integral, energy, electron beam emittance, beta function, and tune in the two transverse planes. The values of constraints found according to the previous expressions are shown in Table 7 and they are fully achievable.

Table 7. Constraints of the field integrals

Integral	Value
I_x	53 G·cm
I_z	9,8 G·cm
J_x	15000 G·cm ²
J_z	8200 G·cm ²

6.2. Variation of first field integral with gap

In figure 11 we show the dependence with the gap of the first vertical field integral I_z . It can be observed that between the working gaps 12.5 and 17.95 mm, the 1st field integral is not within the constraints deduced in the previous section, so correction coils should be used.

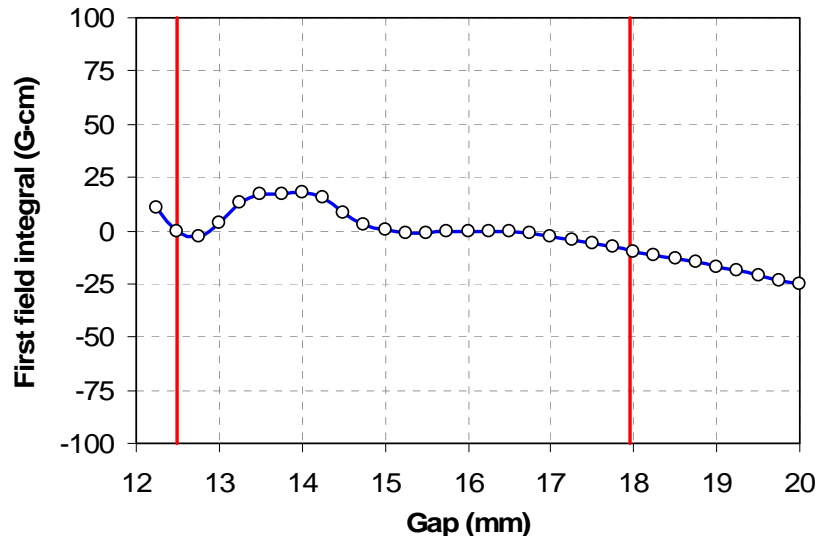


Figure 11. First field integral I_z of the MPW80 versus the gap aperture of the device. In red we mark the operational gaps: 12.5 mm and 17.95 mm.

6.3. Variation of first field integral with gap

In figure 12 we show the dependence with the gap of the vertical magnetic field B_z . According to this evolution, fields below 1 gauss are only achieved for gaps bigger than 860 mm. To reach a field below 10^{-4} the maximum achievable, a gap of 700 mm is required.

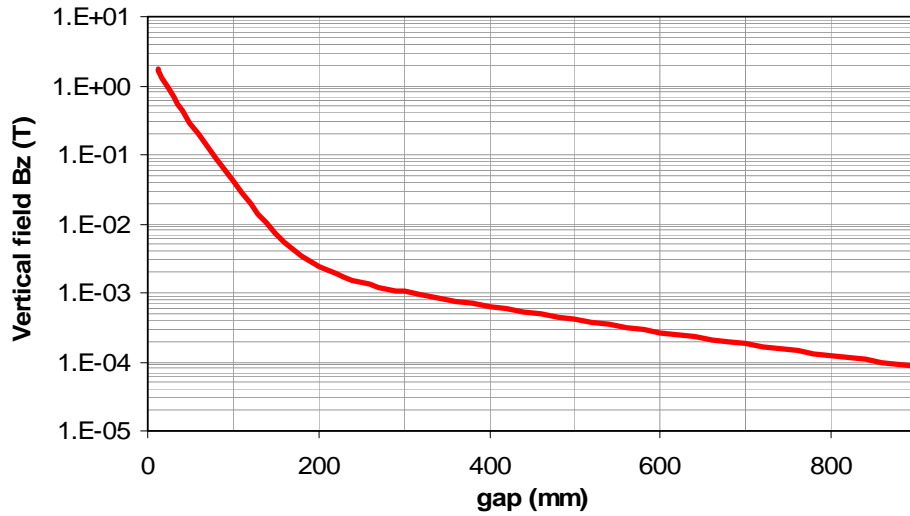


Figure 12. maximum vertical field B_z of the MPW80 versus the gap aperture of the device. To reach 10^{-4} relative to the maximum value at minimum gap it should be opened to 700 mm.

6.4. Maximum field

In Figure 13 we show the evolution of peak magnetic field with gap. Note that from this figure we can extract which should be the operating gaps in order to fulfil the requirements on K defined in table 1.

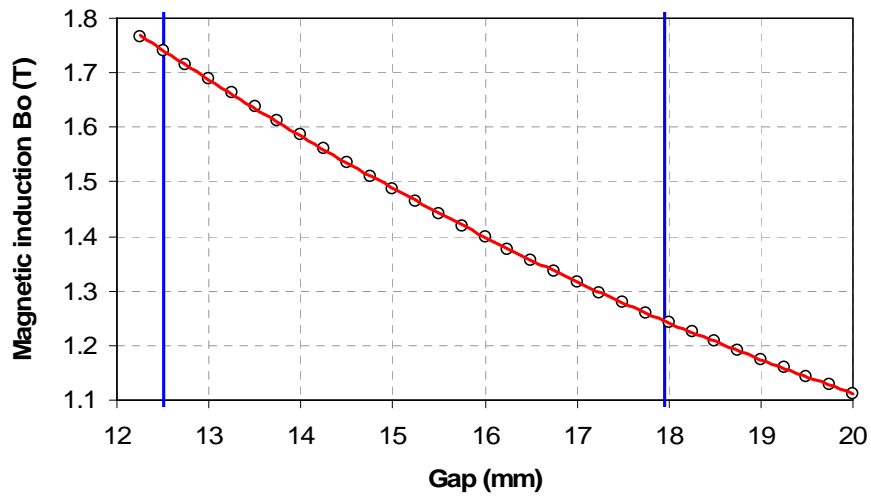


Figure 13. Peak magnetic induction field in the axis of the wiggler MPW80 for each gap aperture. In blue we mark the operational gaps: 12.5 mm and 17.95 mm.

Fitting this result to the well known empirical expression $B_0 = a \cdot \exp\left(b \frac{g}{\lambda_0} + c \left(\frac{g}{\lambda_0}\right)^2\right)$ we find the

following parameters:

a	c	b
4.391	-6.609	4.441

6.5. Forces

The most important force component generated in the wiggler is the vertical one. Because of the high value of the peak field, the forces can achieve up to 5 tones, for the minimum gap aperture of 12.5 mm. The stiffness of the wiggler carriage, as well as the dynamic chain for moving the beams should be designed to cope with these magnitudes. In Figure 14 we show the dependence of forces with the wiggler gap.

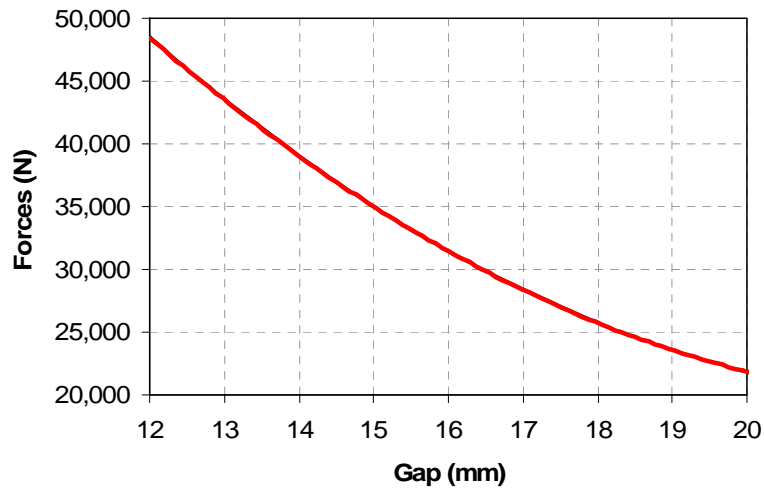


Figure 14. Gap dependence of vertical force generated between both wiggler arrays in W80.

7. Demagnetizing fields

An important issue with high field insertion devices as W80 is that the generated field penetrating the magnetic material can decrease its magnetic performance. In particular, a detailed study should be done

in order to check that the values of demagnetizing field do not exceed the coercivity of the magnetic material. If this happens, the insertion device becomes unfeasible.

In order to evaluate the demagnetizing fields in the worst case, we have used a wiggler model without edge effects, so the calculated field is higher than for the real case.

In Figure 15 we show two cuts of the magnetic block within which we have evaluated the longitudinal component of the demagnetizing field H created by the whole structure.

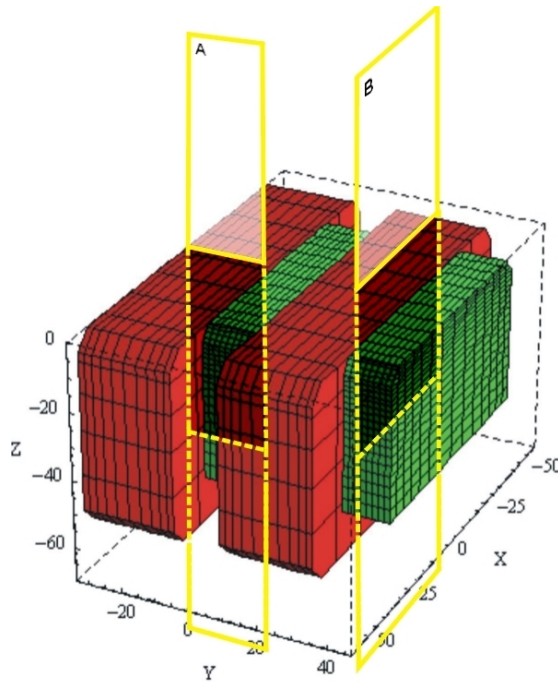


Figure 15. Planes within which demagnetizing field H have been evaluated.

In the plane Y-Z, located at 0.1 mm away from the wiggler axis in X direction, the distribution of longitudinal component demagnetizing field, for a single array is shown in Figure 16 below.

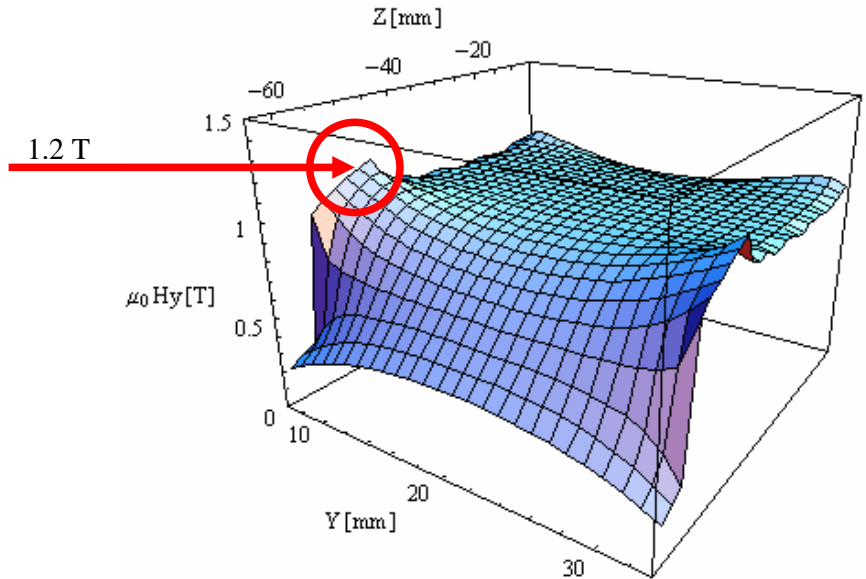


Figure 16. Longitudinal component of demagnetizing field in the Y-Z plane “A”. Please note that colors are not related to the X axis value, they only show geometries. Demagnetizing field is given in T (1 T equivalent to 10 kOe or 795.774 kA/m).

According to Figure 16, the maximum demagnetizing field in the Y-Z plane “A” is 12 kOe (~955 kA/m). However, this field is concentrated in the surface close to the pole edges. The mean demagnetizing field on the plane is 9 kOe (~715 kA/m).

In the plane X-Z, located at 0.1 mm away from the wiggler centre in Y direction, the distribution of longitudinal component demagnetizing field, for a single array is shown in Figure 17 below.

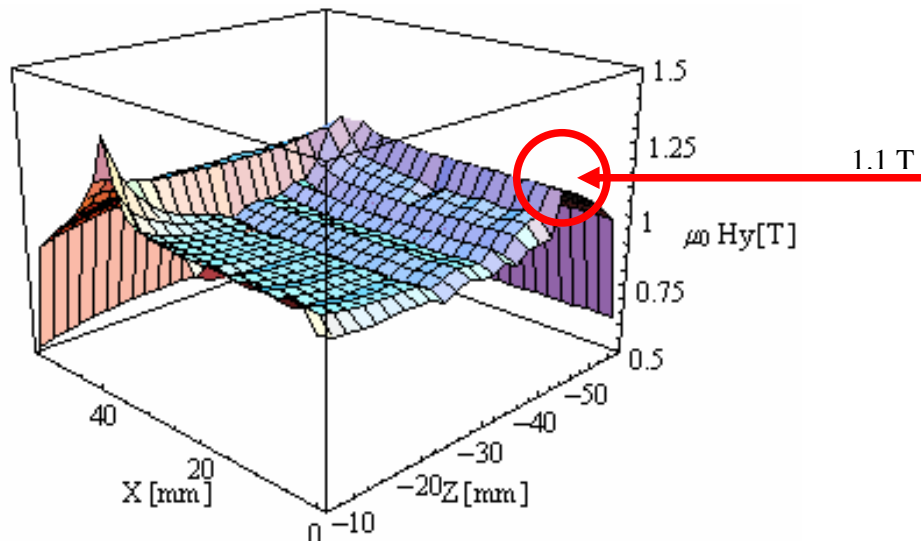


Figure 17. Longitudinal component of demagnetizing field in the X-Z plane “B”.

ALBA Project Document No:	Page: 19/20
AAD-SR-ID-AN-0166	Rev. No. : 1.0

According to Figure 17, the maximum demagnetizing field is concentrated in the surface close to the gap. The mean demagnetizing field on the plane is 11 kOe (~875 kA/m). In general, zones with demagnetizing fields higher than 13 kOe (~1035 kA/m) are located close to the back ends of poles. The calculation of average longitudinal demagnetizing fields in the case of the whole device gives values of 8.6 kOe (~685 kA/m)..

8. Magnetic material

Given the design parameters, we need a magnetic material with a remanence $B_r = 1.4$ T and a coercivity higher than 12 kOe (~955 kA/m). This material exists and can be procured from several suppliers:

- Neomax-50 BH: $B_r = 1.39/1.45$ T, $H_{Jc} = 14$ kOe (~1114 kA/m).
- Vacodym 745 HR: $B_r = 1.40/1.44$ T, $H_{Jc} = 14/15$ kOe (~ 1114/1193 kA/m).
- Nerorem 503 i: $B_r = 1.38/1.41$ T, $H_{Jc} = 13.2/11.9$ kOe (~ 947/1050 kA/m).

9. Tolerances

Wiggler W80 will not be operated in the undulator regime, i. e., from its output, only the smooth part of the spectrum (high energies) will be used. So, the mechanical tolerances are not a big issue in the design, because we are not interested in increase any interference pattern.

For this reason, we fix all the mechanical tolerances in the 0.2 mm range, except in the gap positioning system, where we demand 1 μm in resolution, in order to ensure good repetitivity in the case of working at different operational gaps.

Thus, all deformations of mechanical frame in all directions should guarantee differences less than 0.1 mm between each magnetic arrays and the nominal axis of the device.

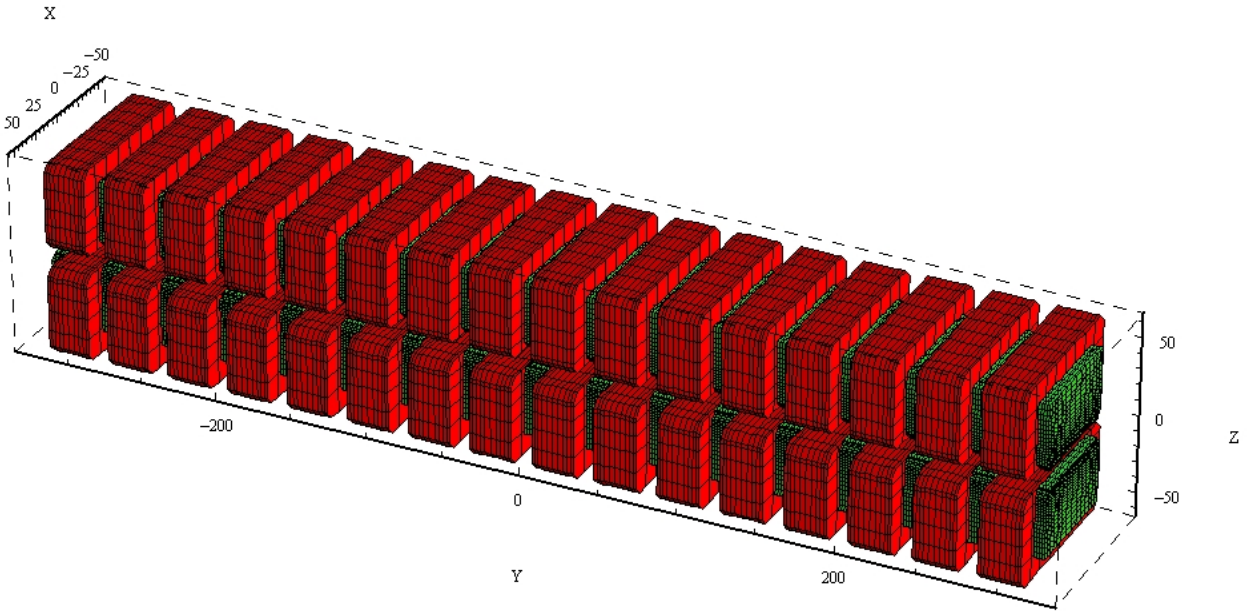
10. Magnetic parameters of wiggler W80

<i>Field Direction</i>	<i>Vertical</i>
<i>Nominal peak on axis field, B_o (gap 12.5 mm)</i>	<i>1.74 T</i>
<i>Nominal peak on axis field, B_o (gap 17.95 mm)</i>	<i>1.25 T</i>
<i>Period length</i>	<i>80 mm</i>
<i>Number of pole pairs @ full field</i>	<i>25</i>
<i>Number of pole pairs @ edge sections</i>	<i>4</i>
<i>Pole length</i>	<i>13.4 mm</i>
<i>Magnetic block length</i>	<i>26.6 mm</i>
<i>Length of magnetic arrangement (not including end sections)</i>	<i>1027 mm</i>
<i>Length of magnetic arrangement (including end sections)</i>	<i>1198 mm</i>
<i>Magnetic length (including stray field $> 5 \cdot 10^{-5}$ T)</i>	<i>1758 mm</i>
<i>Minimum magnetic gap, mm</i>	<i>12.5</i>
<i>Maximum magnetic gap, mm</i>	<i>>300</i>
<i>Transverse field homogeneity at all field levels</i>	$ \Delta B_z / B_z \leq 1\%$ at $x = \pm 20$ mm
<i>Material minimum coercitivity</i>	<i>12 kOe</i>
<i>Gap velocity</i>	<i>Not an issue for this application</i>

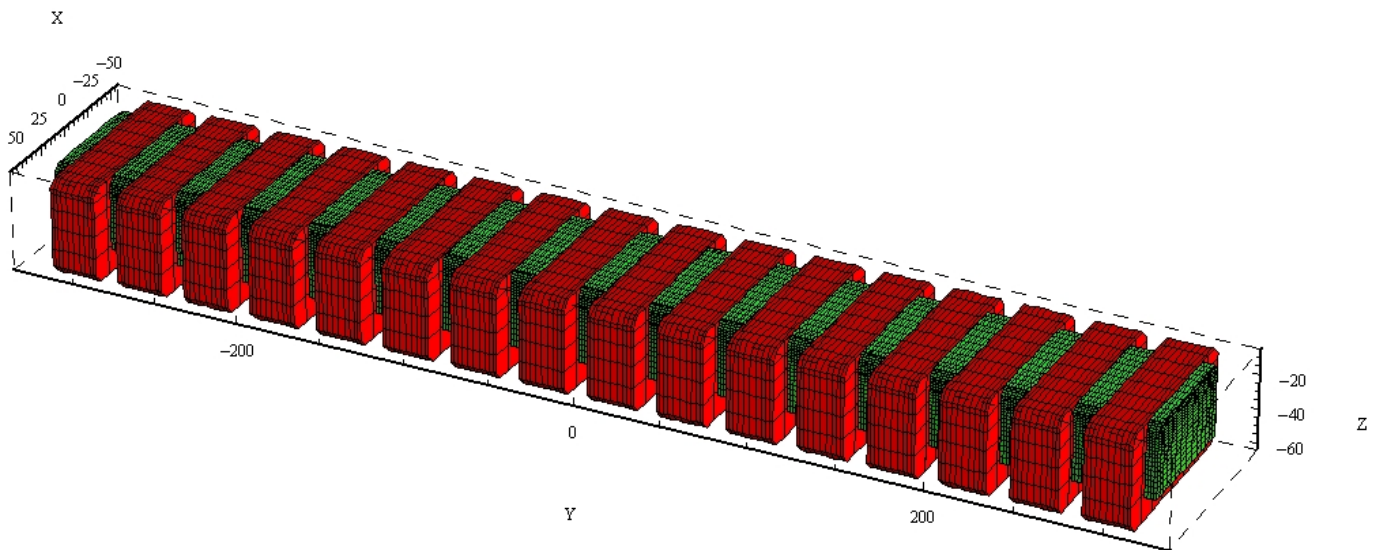
Hybrid MPW80 – CELLS conceptual design.

A) Axis definition.

A.1.) Minimum gap model.

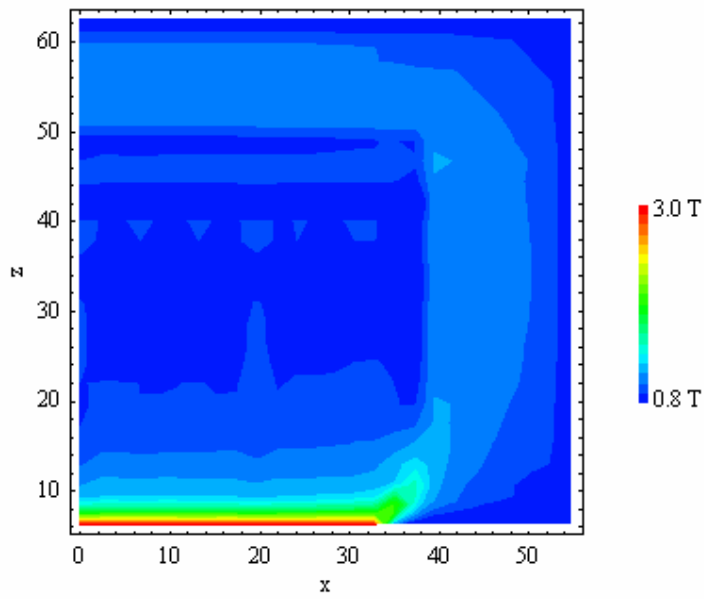


A.2.) Single array mode

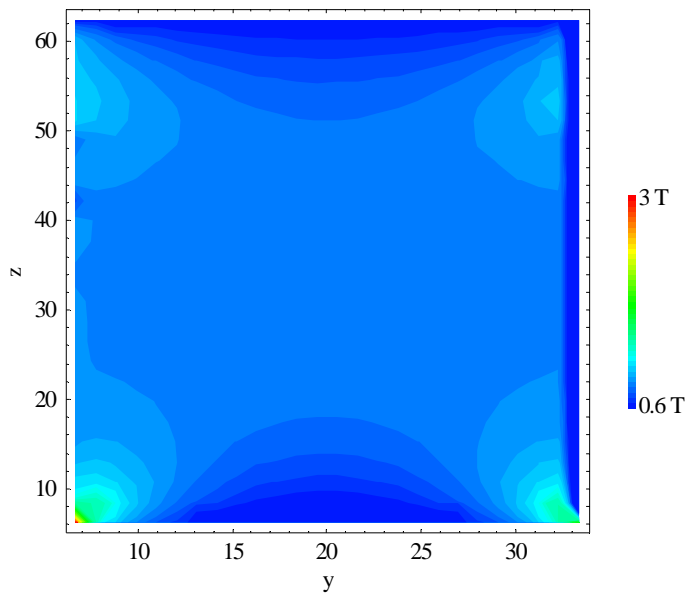


B) De-magnetizing fields for closed-gap device at minimum gap.

B.1.- De-magnetizing field at 0.01 mm below magnetic block / pole interface:



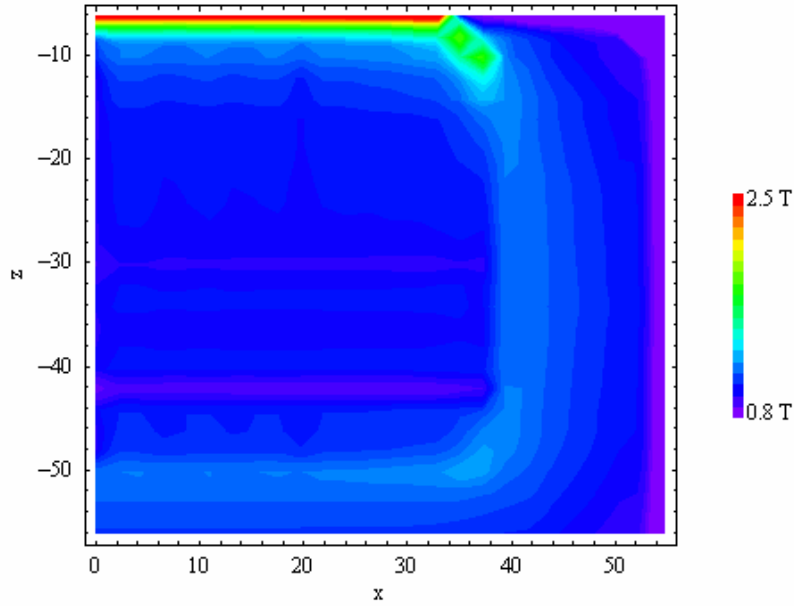
B.2.- De-magnetizing field at $x=0$



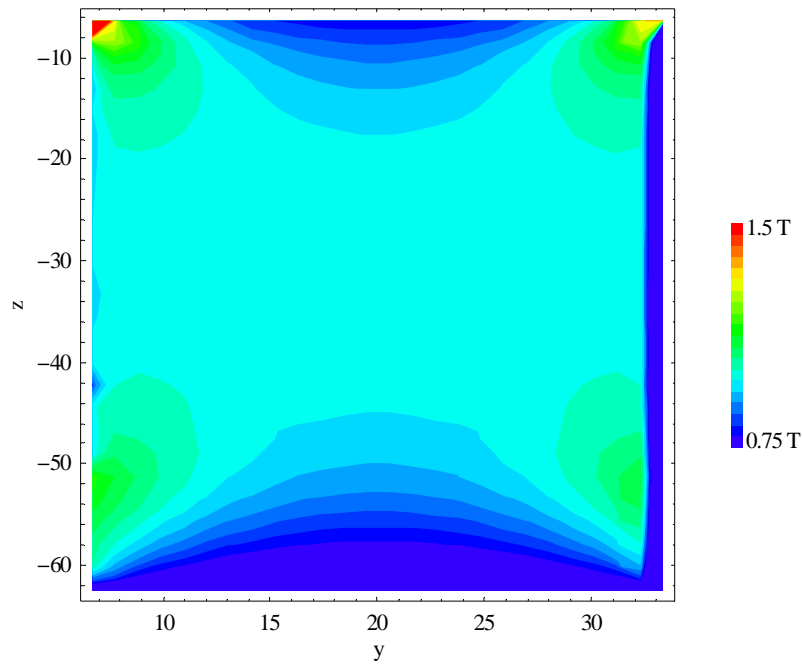
Average de-magnetization field: 0.82 T

C) Worst case: de-magnetizing field for a single array

C.1.- De-magnetizing field at 0.01 mm below magnetic block / pole interface (please note that Z axis is reversed with respect case shown in B.1.):



C.2.- De-magnetizing field at x=0 (Z axis reversed with respect figure in B.2.).



Average de-magnetization field: 1.07 T

Conclusion:

Although De-magnetizing field can reach really very high values (~ 3 T), this only happens in very localized regions of magnetic blocks. So, may be the model is still “feasible”.

The only objection that can be done is a practical issue: may be when assembling the wiggler, the de-magnetizing fields can be so high that a 1.4 T of coercitivity is not enough to guarantee the performance.

Calculations were done with RADIA 4.117, using the notebook:

[DemagnetizingFields\(HY\)-wiggler80-16-05-07-bis.nb](#)

Josep Campmany
ALBA-CELLS, 16/05/07